THE JOURNAL OF PHYSICAL CHEMISTRY B

Article

pubs.acs.org/JPCB

Transferable Potentials for Phase Equilibria–United Atom Description of Five- and Six-Membered Cyclic Alkanes and Ethers

Samuel J. Keasler,[†] Sophia M. Charan,[†] Collin D. Wick,[‡] Ioannis G. Economou,[§] and J. Ilja Siepmann*,[†]

[†]Departments of Chemistry and of Chemical Engineering and Materials Science and Chemical Theory Center, University of Minnesota, 207 Pleasant Street SE, Minneapolis, Minnesota 55455, United States

[‡]Department of Chemistry, Louisiana Tech University, P.O. Box 10348, Ruston, Louisiana 71270, United States

[§]Department of Chemical Engineering, The Petroleum Institute, P.O. Box 2533, Abu Dhabi, United Arab Emirates

Supporting Information

ABSTRACT: While the transferable potentials for phase equilibria–united atom (TraPPE–UA) force field has generally been successful at providing parameters that are highly transferable between different molecules, the polarity and polarizability of a given functional group can be significantly perturbed in small cyclic structures, which limits the transferability of parameters obtained for linear molecules. This has motivated us to develop a version of the TraPPE–UA force field specifically for five- and six-membered cyclic alkanes and ethers. The Lennard-Jones parameters for the methylene group obtained from cyclic alkanes are transferred to the ethers for each ring size, and those for the oxygen atom are common to all compounds for a given ring size. However, the partial charges are molecule specific and parametrized using liquid-phase dielectric constants. This model yields accurate saturated liquid densities and vapor pressures, critical temperatures and densities, normal boiling points, heat capacities, and isothermal compressibilities for the following molecules: cyclopentane, tetrahydrofuran, 1,3-dioxolane, cyclohexane, oxane, 1,4-dioxane, 1,3-dioxane, and 1,3,5-trioxane. The azeotropic behavior and separation factor for the binary mixtures of 1,3-dioxolane/cyclohexane and ethanol/1,4-dioxane are qualitively reproduced.

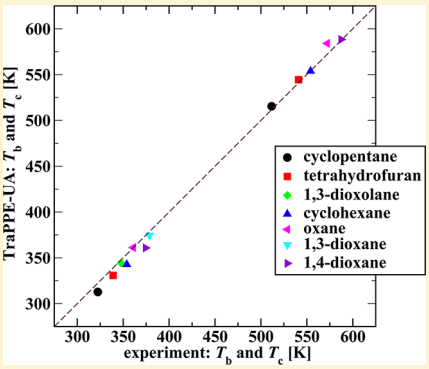

1. INTRODUCTION

Small cyclic alkanes and ethers are an important class of molecules used in a wide variety of industrial applications. Cyclopentane, cyclohexane, and their derivatives are significant components of crude oil.[1] Furthermore, cyclic ethers are an important building block for sugars and many natural and pharmaceutical compounds. With rapid improvements in simulation algorithms and increases in computer power over the last few decades, molecular simulations have become a valuable tool for predicting the properties of complex chemical systems and can provide valuable insight into the microscopic origin of macroscopic measurables. The accuracy of a molecular simulation is determined by the quality of the potential energy functions or force field used to describe interactions of the atoms and molecules in the system.[2] Thus, an ongoing goal of the research community has been the development of accurate force fields.[3−8]

To this extent, our group has developed the transferable potentials for phase equilibria (TraPPE) force field by fitting the parameters to (mostly vapor–liquid) phase coexistence properties over a wide range of temperatures. One of the most important requirements for these potentials is that they be transferable, meaning that the parameters used to describe a particular functional group should accurately represent the interactions of that group in molecules and environments beyond those for which it was explicitly parametrized. This approach has now been successfully applied to a broad range of functional groups.[9−19]

The previous work has been quite successful at producing force fields that are both accurate and transferable. On the basis of this success, one might hope that the parameters used for acyclic alkanes and ethers would be transferable to cyclic molecules. However, calculations for the cyclic alkanes show limited transferability for small cyclic molecules,[20] and the TraPPE-UA parameters for linear ethers have been shown to provide a poor description of the phase equilibria for ethylene oxide[21] and 1,4-dioxane.[22] The constraints imposed by the cyclic structure, particularly for the smaller rings, can significantly change the geometry (bending angles and to a lesser extent bond lengths) compared to the acyclic compounds. This ring strain leads to changes in the polarizability and molecular charge distribution.[23,24] Furthermore, the errors in the densities and critical properties for cyclic alkanes have been found to increase with decreasing ring size for the same parameter set,[20] indicating that the magnitude of this effect may depend significantly on the number of carbon and oxygen atoms in the ring.

Received: March 28, 2012
Revised: August 13, 2012
Published: August 20, 2012

Several force fields for five- and six-membered rings have been proposed in the literature. A number of models for cyclic alkanes, particularly cyclohexane, have been developed[25−28] including a Buckingham exponential-6 model[25] and an anisotropic united-atom model[26] that can accurately reproduce the vapor−liquid equilibria. A few simulations of tetrahydrofuran (THF) have been performed,[29,30] using models adapted from the OPLS[31] and AMBER[3] force fields for linear ethers, and several THF force fields have been been examined by Girard and Müller-Plathe.[32] There have also been a few models developed for 1,4-dioxane,[22,33,34] including one fit to the vapor−liquid coexistence curve.[22]

Despite significant efforts to develop models for single molecules or for a small class of molecules, there has been little work devoted to finding more general, transferable parameters for cyclic molecules. This has motivated us to fit new parameter sets for united-atom (UA) representations of cyclic alkanes and ethers, one for five-membered rings and another for six-membered rings. The parameters for the five-membered rings were fitted to give good agreement with vapor−liquid equilibria for cyclopentane, THF, and 1,3-dioxolane, while the parameters for six-membered rings were fitted to data for cyclohexane, oxane, 1,4-dioxane, 1,3-dioxane, and 1,3,5-trioxane.

2. FORCE-FIELD DEVELOPMENT

The TraPPE force field uses Lennard-Jones (LJ) and Coulomb potentials to describe the nonbonded interactions

$$U(r_{ij}) = 4\epsilon_{ij}\left[\left(\frac{\sigma_{ij}}{r_{ij}}\right)^{12} - \left(\frac{\sigma_{ij}}{r_{ij}}\right)^{6}\right] + \frac{q_i q_j}{4\pi\epsilon_0 r_{ij}} \quad (1)$$

where r_{ij}, σ_{ij}, ε_{ij}, q_i, q_j, and ε_0 are the separation between interaction sites i and j, the LJ diameter and well depth, the partial charges on interaction sites i and j, and the permittivity of vacuum, respectively. Lennard-Jones parameters for unlike interactions are obtained using the Lorentz−Berthelot combining rules.[35]

In the TraPPE−UA force field for linear ethers,[14] partial charges are placed on the interactions sites of the oxygen atoms and the CH_2 united atoms bonded directly to the oxygen atom. While there is likely a small partial charge on the β-carbons as well, this will generally have a relatively small impact on the phase equilibria of linear ethers and has been negleced. For cyclic ethers, the constrained geometry of the molecule results in the charge on the β-carbons having a significant effect on the molecular dipole moment. For example, density functional theory (DFT) calculations of the global energy minimum at the B3PW91/6-31++G(d,p) level[36] yield a dipole moment of 2.042 D for THF and 1.381 D for diethyl ether. To account for this effect, small partial charges were placed on the β-carbons (+0.045|e| for THF and +0.050|e| for oxane and 1,3-dioxane). For all but 1,4-dioxane, the partial charges were obtained by fitting to the liquid-phase dielectric constant using the TraPPE−UA charges for linear ethers as the initial guess. Such a procedure could not be used for 1,4-dioxane as the molecular dipole is much smaller than that of the other oxygenated molecules and it would be impossible for a fixed-charge force field to reproduce the dielectric constant without resorting to extremely large charges. For this molecule, the oxygen and α-carbon charges were chosen to be between those found for oxane and 1,3,5-trioxane, though somewhat closer to 1,3,5-trioxane, as Mulliken charges[37] taken from B3PW91/6-31++G(d,p) calculations for the isolated molecules were substantially larger for oxane than either of the other two molecules.

This charge fitting procedure gives charges that provide an effective description of the liquid phase properties. By fitting to the dielectric constant, the contribution from electronic polarizability in the liquid phase is implicitly accounted for, which leads to charges that are somewhat too high in the vapor phase. Greater importance was placed on the liquid phase for these models to describe solution properties, such as solvation free energies and liquid−liquid equilibria, with better accuracy.

The LJ parameters were fit in a stepwise manner. The CH_2 parameters for the five- and six-membered rings were obtained by fitting to the saturated liquid densities, vapor pressures, and critical temperatures for cyclopentane and cyclohexane, respectively. These LJ parameters were then transferred to the cyclic ethers. For the five-membered rings, the oxygen parameters were obtained by fitting to the saturated liquid densities, vapor pressures, and critical temperature for THF, along with the vapor pressure and one room temperature density point for 1,3-dioxolane. For the six-membered rings, the oxygen parameters were fit to the same data for oxane, 1,4-dioxane, 1,3-dioxane, and 1,3,5-trioxane, except that experimental values of the saturated liquid densities for oxane and 1,3-dioxane and of the critical properties for 1,3,5-trioxane and 1,3-dioxane could not be found in the literature. As for 1,3-dioxolane, the liquid densities for oxane and 1,3-dioxane were compared to one data point near room temperature.

The LJ parameters and partial charges used in this study are summarized in Table 1. Compared to the parameters for linear molecules, the LJ diameters for the CH_2 beads are slightly smaller, and the well depths are increased, in both cases by a larger degree for the five-membered rings than for the six-

Table 1. TraPPE−UA Force Field Parameters for Nonbonded Interactions

ring size − bead	σ [Å]	ε/k_B [K]
5 − CH_2	3.88	56.3
5 − O	2.20	190
6 − CH_2	3.91	52.5
6 − O	2.39	155
molecule	**bead**	q [|e|]
cyclopentane	CH_2	0.000
THF	O	−0.410
THF	$CH_2(\alpha)$	0.160
THF	$CH_2(\beta)$	0.045
1,3-dioxolane	O	−0.425
1,3-dioxolane	CH_2 (O−CH_2−O)	0.360
1,3-dioxolane	$CH_2(\alpha)$	0.245
cyclohexane	CH_2	0.000
oxane	O	−0.440
oxane	$CH_2(\alpha)$	0.170
oxane	$CH_2(\beta)$	0.050
1,4-dioxane	O	−0.380
1,4-dioxane	CH_2	0.190
1,3-dioxane	O	−0.395
1,3-dioxane	CH_2 (O−CH_2−O)	0.360
1,3-dioxane	$CH_2(\alpha)$	0.190
1,3-dioxane	$CH_2(\beta)$	0.050
1,3,5-trioxane	O	−0.360
1,3,5-trioxane	CH_2	0.360

dx.doi.org/10.1021/jp302975c | J. Phys. Chem. B 2012, 116, 11234−11246

membered rings. For the oxygen parameters, the length parameter is also smaller than the parameter in linear ethers (by a larger amount than the CH_2 parameter), and the well depth is considerably larger (over twice the value found for the linear ethers). The magnitude of the partial charges on the oxygen atom and α-CH_2 group is smaller than for the linear ethers. The geometry of cyclic molecules constrains the more polarizable carbon−hydrogen bonds and oxygen lone pairs that are implicitly modeled in the united atom description to be on the perimeter of the molecule where accessibility differs from linear molecules. This is likely the major physical reason for the increased well depth and decreased diameter. The magnitude of this effect is larger for the smaller, more rigid five-membered rings. In addition, the parameters for the oxygen may be more significantly perturbed due to the constraint of CH_2 transferability. The α-carbon group represents the electrostatic interactions of not only the valence electrons in the C−H bonds but also part of the valence electrons in the C−C and C−O bonds. Thus, the oxygen parameter also accounts for the change of a C−CH_2−C unit to a C−CH_2−O unit.

As is customary for the TraPPE force field, fixed bond lengths are used. If desired for molecular dynamics simulations, harmonic bond stretching constants from other force fields[3,5] can be used. Beads separated by two bonds interact by a harmonic bending potential of the form

$$U_{\text{bend}}(\theta) = \frac{k_\theta}{2}(\theta - \theta_0)^2 \tag{2}$$

Bending force constants were taken from the TraPPE−UA force field for *n*-alkanes and ethers. For the six-membered rings, DFT calculations at the B3PW91/6-31++G(d,p) level did not show any large systematic deviations from the equilibrium angles used in the linear molecules, and these parameters were transferred directly to the cyclic molecules. The only bond angle not available from previous versions of the TraPPE force field was the O−C−O angle for which the bending angle and the force constant were both taken from the OPLS-AA force field,[4] which has an equilibrium angle almost exactly equal to the DFT value for 1,3,5-trioxane and is smaller by about 1.5° than the value in 1,3-dioxane. For the five-membered rings, the equilibrium bond angles of the linear analogues were significantly different from the DFT values for the cyclic molecules; so to accurately describe the molecular shape, the equilibrium angles were adjusted to be close to the values from the optimized structures. The bond bending parameters are summarized in Table 2.

Interactions between beads separated by three bonds in the TraPPE−UA force field are generally represented by a cosine series of the form

Table 2. Equilibrium Bond Angles and Force Constants

ring size	angle	θ_0 [degrees]	k_θ/k_B [K rad^{-2}]	reference
5	C−C−C	105.50	62500	this work
5	C−C−O	108.50	50300	this work
5	C−O−C	112.00	60400	this work
5	O−C−O	109.00	93200	this work
6	C−C−C	114.00	62500	9
6	C−C−O	112.00	50300	14
6	C−O−C	112.00	60400	14
6	O−C−O	111.55	93200	31

$$V_{\text{tors}}(\phi) = c_0 + c_1[\cos(\phi)] + c_2[\cos(2\phi)] + c_3[\cos(3\phi)] \tag{3}$$

An examination of the potentials for the cyclic alkanes and ethers showed that the torsional energies obtained from DFT calculations at the B3PW91/6-31++G(d,p) level were poorly reproduced by the parameters for linear molecules. A new set of torsional potentials was obtained for the five-membered rings by fitting to a scan around each unique torsion type in cyclopentane, THF, and 1,3-dioxolane. For cases where two molecules contained the same torsion type (i.e., C−C−C−C in cyclopentane and THF), separate scans were obtained for each molecule. The scans were performed in 5° increments from −60° to 60° where all other degrees of freedom (including the unconstrained torsions) were allowed to relax. The range was restricted because larger values of the dihedral angles produced very high energies that made it difficult to accurately fit the more important, lower-energy portion of the torsional potential energy surface. For the six-membered rings, scans of each torsion type in cyclohexane, oxane, 1,4-dioxane, 1,3-dioxane, and 1,3,5-trioxane were included in the fitting procedure where the larger rings are more flexible, allowing scans from −85° to 85° to be used.

When using a relaxed torsional scan, all of the dihedral angles can change at each step, which is particularly important for these small cyclic molecules where the geometry is constrained and the various intramolecular degrees of freedom are strongly coupled. This makes it difficult to decompose the energy change into the contributions of different torsion types. Furthermore, several of the torsion types appear in more than one molecule, and where possible, a compromise set of parameters that fits all scans as well as possible is preferred. Therefore, all of the relevant torsional potentials were simultaneously fit to all the available torsional scans. We used a Monte Carlo algorithm with simulated annealing to find the values for the torsional parameters that minimize the Boltzmann weighted unsigned deviation from all seven torsional scans. Monte Carlo moves were performed on the torsional parameters and accepted with a probability

$$P_{\text{acc}} = \min\left\{1, \exp\left[-\frac{\sum_{i=1}^{N_{\text{conf}}} |\Delta\Delta U_i| \exp(-\Delta U_{i,\text{DFT}}/k_B T_{\text{weight}})}{N_{\text{conf}} k_B T_{\text{anneal}}}\right]\right\} \tag{4}$$

where the summation runs over all the relevant conformations, N_{conf}, that can arise from different torsion scans and different molecules; $\Delta\Delta U_i$ is the difference between the corrected trial TraPPE−UA energy, $\Delta U_{i,\text{TraPPE−UA}}$, and the corrected DFT energy, $\Delta U_{i,\text{DFT}}$, for a particular configuration with the latter being the difference in DFT energies for this conformation and the lowest energy conformation corrected by the difference in the TraPPE angle bending energy for these two conformations. The corrected TraPPE−UA energy is also taken with respect to the same lowest-energy conformation (and excludes angle bending energies and would exclude nonbonded interactions for larger molecules).

Two different temperatures are used in the fitting procedure. T_{anneal} is the temperature used in the simulated annealing run. Its value is initially chosen to be sufficiently large so that nearly all of the Monte Carlo moves are accepted. This helps to ensure

that the final parameters are not sensitive to the initial guess. The temperature is reduced periodically during the fit until the acceptance rate is around 5% or less. T_{weight} is a parameter controlling how heavily the fit is weighted toward low-energy configurations. For both of the fits presented here, T_{weight} is set to 10^4 K. A lower value was found to only slightly improve the fit to the low-energy data but led to a considerably worse fit for the higher-energy points. The basic structure of this fitting algorithm is similar to that proposed by Guvench and MacKerell.[38] However, Boltzmann weighting is a more systematic approach than manually assigning an arbitrary, higher weight to the low-energy points, and with the exception of a few outlying points generally provides a good fit to both low- and high-energy structures. Furthermore, the fit is performed here simultaneously to multiple molecules.

Comparisons of the corrected TraPPE−UA energies obtained from this fitting procedure and the corrected DFT energies for the five- and six-membered rings are presented in Figure 1. The DFT energies are fit quite well overall by the

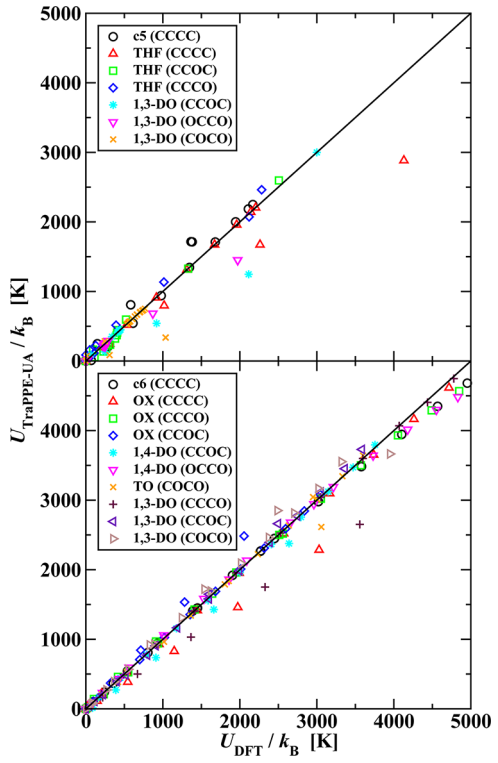

Figure 1. Scatter plots of the TraPPE−UA torsional energies versus the DFT energies for the five-membered rings (top; DO = dioxolane) and six-membered rings (bottom; OX = oxane, DO = dioxane, TO = trioxane). The solid line indicates perfect agreement.

TraPPE−UA torsional potential, particularly at low energies. For both ring sizes, deviations at low energy are typically due to a slight error in the conformation of the energy minimum, though the general shape of the dihedral surfaces is very well described. The TraPPE−UA torsional parameters are summarized in Table 3. The constrained structure of the cyclic molecules leads to substantially stiffer torsional potentials than are observed for acyclic molecules, and the potentials for the five-membered rings are stiffer than for the six-membered rings, also due to the more rigid structure for the smaller ring.

Table 3. Torsional Parameters

ring size	torsion type	c_0/k_B [K]	c_1/k_B [K]	c_2/k_B [K]	c_3/k_B [K]
5	C−C−C−C	31394	45914	16518	1496
5	C−C−O−C	21933	40808	16851	2392
5	C−C−C−O	21903	24297	8147	246
5	O−C−C−O	20131	45634	17785	2100
5	C−O−C−O	20469	15333	5776	181
6	C−C−C−C	5073	6840	3509	63
6	C−C−O−C	7037	14958	7606	1546
6	C−C−C−O	7031	5218	2287	−569
6	O−C−C−O	13537	10876	5223	−123
6	C−O−C−O	11721	17718	8879	1584

3. SIMULATION DETAILS

To compute the vapor−liquid coexistence curves (VLCC), the *NVT* Gibbs ensemble[39,40] was used. In this ensemble, two separate simulation boxes with a constant total number of molecules and constant total volume are kept in thermodynamic contact but have no explicit interface. For these simulations, the chemical potential in the two phases is equalized by performing configurational-bias Monte Carlo particle transfer moves between the two boxes during which the ring conformation is held rigid but multiple trial locations and orientations are explored.[10,41−43] The pressure of the two phases is equalized by performing volume exchange moves.[40] The conformational (or vibrational) degrees of freedom of the rings are sampled separately using self-adapting fixed end point configurational-bias Monte Carlo (SAFE-CBMC) moves.[44] Translational and rotational moves with the conformation held rigid are performed to sample the remaining degrees of freedom.

For the unary and binary Gibbs ensemble simulations, system sizes of 370 and 500 molecules were used. A spherical cutoff of r_{cut} = 14 Å with analytic tail corrections[45] was employed for the LJ interactions. The Coulomb interactions were computed using the Ewald summation technique with tin foil boundary conditions.[46−48] The real-space cutoff was equal to r_{cut}, and the Ewald sum convergence parameter was set to $3.5/r_{cut}$. Liquid-phase simulation box sizes were larger than twice r_{cut}. Vapor-phase box sizes were adjusted so that on average at least 30 molecules were present in the vapor phase. In cases where the saturated vapor pressure is low, the vapor-phase box must be quite large for 30 molecules to be present. For large simulation boxes, the Ewald sum becomes quite expensive; hence, once the vapor box length exceeds 50 Å, we set r_{cut} to be equal to a fixed value of ≈40% of the average box length, which is sufficiently small so that fluctuations in the volume are not encountered that would reduce the box length to a size smaller than twice of the cutoff. As there are few molecules in the vapor phase, this increases the efficiency by reducing the number of reciprocal-space vectors used in the Ewald sum.

For unary systems, the simulations were equilibrated for 10^5 Monte Carlo cycles, and the production runs consisted of 2.5×10^5 Monte Carlo cycles. A Monte Carlo cycle consists of N Monte Carlo moves where N is the number of molecules in the system. The probabilities of performing volume, particle transfer, SAFE-CBMC regrowth, and translational and rotational moves are 0.1%, 9.9%, 30%, 30%, and 30%, respectively. The move type and the molecule to be moved are selected at random. For all unary Gibbs ensemble simulations, structural analysis was performed at a temperature point within 10 K of

dx.doi.org/10.1021/jp302975c | J. Phys. Chem. B 2012, 116, 11234−11246

400 K. The critical temperature, T_c, and critical density, ρ_c, were estimated using fits of the coexistence densities to the scaling law[49] with a critical exponent of 0.326 and the law of rectilinear diameters.[50] The normal boiling points (T_{boil}) were calculated using the Clausius−Clapeyron equation.[51] Only the four highest temperatures were used to determine the critical point, and the two temperatures closest to the boiling temperature were used to determine the normal boiling point.

To calculate the dielectric constants, the near-ambient density (the temperature is set to the value used for the experimental measurements and is close to 298 K and p = 1 atm) was determined first for each dipolar molecule from simulations with N = 300 in the isobaric−isothermal ensemble.[52] Simulations in the NVT ensemble were then performed at this average density to obtain the dielectric constant from the fluctuations in the system dipole[48] using

$$\varepsilon = 1 + \frac{4\pi}{3Vk_BT}[\langle M^2\rangle - \langle M\rangle^2] \tag{5}$$

where M is the total system dipole moment and V is the volume. The dielectric constant is calculated over eight independent simulations consisting each of 5 × 10^5 Monte Carlo cycles. The moves were divided evenly between translations, rotations, and SAFE-CBMC regrowth moves in the NVT simulations, while in the NpT simulations there was a 0.1% probability of performing a volume move, with the rest of the moves divided evenly between the other three types.

Additionally, eight independent NpT simulations of 1 × 10^5 Monte Carlo cycles were performed to compute the isothermal compressibilities and constant-pressure heat capacities. These simulations were performed at 300 K and the saturated vapor pressure for the model. The compressibility can be calculated from the fluctuation in the system volume using[53]

$$\kappa = \frac{1}{k_BT\langle V\rangle}[\langle V^2\rangle - \langle V\rangle^2] \tag{6}$$

The heat capacity can be computed from fluctuations in the enthalpy. However, using the enthalpy directly from a classical simulation assumes that all of the vibrational degrees of freedom can be treated clasically, which is a poor assumption for vibrations at most temperatures of interest.[53] Instead, the heat capcaity is divided into an ideal part and a residual part, where the residual part is computed from

$$C_p^{res} = \left(\frac{\partial\langle H_{inter}\rangle}{\partial T}\right)_p - Nk_B \tag{7}$$

This residual part can be computed from the simulations using

$$C_p^{res} + Nk_B = \frac{1}{k_BT^2}(\langle H_{inter}H_{full}\rangle - \langle H_{inter}\rangle\langle H_{full}\rangle) \tag{8}$$

where H_{full} is the enthalpy of the system considering all intramolecular interactions and H_{inter} excludes all intramolecular energy contributions. The ideal part can be computed using

$$C_p^{ideal} = 4Nk_B + Nk_B\sum_{j=1}^{3n-6}\left(\frac{h\nu_j}{k_BT}\right)^2\frac{\exp(h\nu_j/k_BT)}{[\exp(h\nu_j/k_BT) - 1]^2} \tag{9}$$

where the $4Nk_B$ contribution accounts for the translational and rotational contributions and volume fluctuations, and the frequencies were determined from B3PW91/6-31+G(d,p) calculations and were scaled by a factor of 0.960. A sightly smaller basis set was used for these calculations than was used for other electronic structure calculations because of the availability of empirical scaling factors for this functional and basis set combination.[54]

The vapor−liquid equilibria for the binary mixtures of cyclohexane/1,3-dioxolane and ethanol/1,4-dioxane were also studied. The first case provided an opportunity to examine the interactions between both five- and six-membered ring parameter sets as well as between a nonpolar and a polar molecule. The second case was chosen to provide insight into the hydrogen bond acceptor ability of the oxygen atom in a cyclic ether. For these mixtures, eight independent NVT Gibbs ensemble simulations were performed. For each simulation, 10^5 Monte Carlo cycles were used for equilibration, and 2 × 10^5 Monte Carlo cycles were used for production with the move probabilities the same as for the unary Gibbs ensemble simulations.

The statistical uncertainties in the VLCC properties for neat systems were estimated by dividing the corresponding production runs into ten blocks and calculating the standard error of the mean for these blocks. For the dielectric constants and the binary systems, the data from the independent simulations were used to estimate the standard error of the mean. The uncertainties in the critical properties and normal boiling points are reported as 95% confidence intervals.

4. RESULTS AND DISCUSSION

4.1. Dielectric Constants. To fit the partial charges for the oxygenated molecules, liquid-phase dielectric constants were calculated for the dipolar molecules and compared to the experimental values for THF,[55] 1,3-dioxolane,[56] oxane,[55] 1,3-dioxane,[57] and 1,3,5-trioxane.[55] As an initial guess, it was assumed that the Lennard-Jones parameters for the oxygen atoms could be obtained by scaling σ and ε from the TraPPE−UA model for acyclic ethers by the same ratio as the cyclopentane and cyclohexane LJ parameters for the methylene group were scaled relative to the acyclic alkanes. The initial guesses for the partial charges were taken from the TraPPE−UA model for linear ethers and from electronic structure calculations for the β-carbons.

The process of fitting the partial charges was an iterative one. First, the specific density of a given compound was determined for a model with the initial guesses of the LJ parameters for the oxygen atoms and for the partial charges. Then the dielectric constant for this initial model was computed, followed by adjustments (every time scaling all partial charges by a common factor) that were made until the predicted dielectric constant matched the corresponding experimental value. This set of partial charges was then used for VLCC calculations, and the LJ parameters for the oxygen atom were adjusted to yield a good match to the experimental VLCC data.

The average density and the dielectric constant were recomputed using these LJ parameters and, largely because our initial guess for the oxygen LJ parameters turned out to be poor, a second iteration was required in which the partial charges were readjusted to fit the dielectric constants (now requiring only small adjustments). Then the LJ parameters for oxygen were optimized again to the VLCC data. The values of the dielectric constants obtained with the final parameter set, along with the experimental values, are listed in Table 4. In general, the agreement is quite good. The only significant

Table 4. Comparison of Dielectric Constants Measured Experimentally[55−57] and Predicted by Simulation

molecule	$\varepsilon_{\text{TraPPE–UA}}$	$\varepsilon_{\text{expt}}$
THF	7.2 ± 0.1	7.46
THF Briggs	4.7 ± 0.1	7.46
THF Girard	16.9 ± 0.3	7.46
THF Helfrich	5.0 ± 0.1	7.46
1,3-dioxolane	7.1 ± 0.1	7.00
oxane	5.7 ± 0.1	5.60
1,3-dioxane	13.9 ± 0.3	13.9
1,3,5-trioxane	17.8 ± 0.5	15.55

deviation is observed for 1,3,5-trioxane; however, for this molecule, it was found that the dielectric constant is very sensitive to small changes in both the partial charges and the LJ parameters, and further iterations were unlikely to significantly improve the description of the charge distribution.

For comparison, dielectric constants have also been computed for the three UA models for THF considered by Girard and Müller-Plathe.[32] These include an adaptation of the OPLS model from Briggs et al. (referred to as the Briggs model),[58] a model from Helfrich and Hentschke fit to diffusion constants (referred to as the Helfrich model),[30] and an adaptation of the Helfrich model by Girard and Müller-Plathe which will be referred to as the Girard model. These models do not perform as well as the TraPPE–UA model for the permittivity, with the Briggs and Helfrich models both underprediciting the dielectric constant by more than 30% and the Girard model predicting a value more than twice as large as the experimental one.

4.2. Vapor–Liquid Equilibria and Structural Data for Five-Membered Rings. The VLCCs, along with literature data for cyclopentane[59] and THF,[60] are shown in Figure 2. For the oxygenated rings, few experimental density data except at low temperature were available, and in some instances,

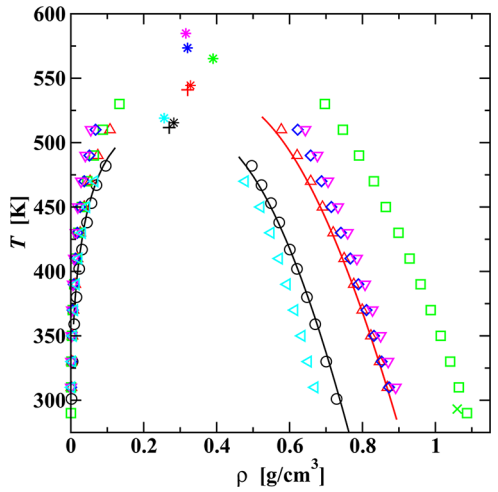

Figure 2. Vapor–liquid coexistence curves predicted by the TraPPE–UA force field for cyclopentane, THF, and 1,3-dioxolane are shown as black circles, red triangles, and green squares, respectively, while the corresponding experimental data[59,60] are shown as solid lines. Results for THF using the Briggs, Girard, and Helfrich models are shown as blue diamonds, magenta down triangles, and cyan left triangles, respectively. Predicted and experimental critical points[61] are shown as stars and plus signs, respectively. The experimental liquid density of 1,3-dioxolane at 293.15 K[55] is indicated as a green cross.

correlations from Yaws[60] have been used to fit the liquid densities. The liquid densities generally agree very well with the available data, with average deviations less than 1%. For 1,3-dioxolane, the liquid density at 293.15 K is slightly overestimated, but the selected oxygen parameters work very well for THF. The Briggs and Girard models give good agreement with the low-temperature liquid density of THF but yield densities that are too high at elevated temperatures, whereas the Helfrich model, that was not fit to any phase coexistence properties, severely underpredicts the liquid density over the entire range of temperatures.

Clausius–Clapeyron plots of the saturated vapor pressures are compared to the experimental data[59,61,62] in Figure 3. The

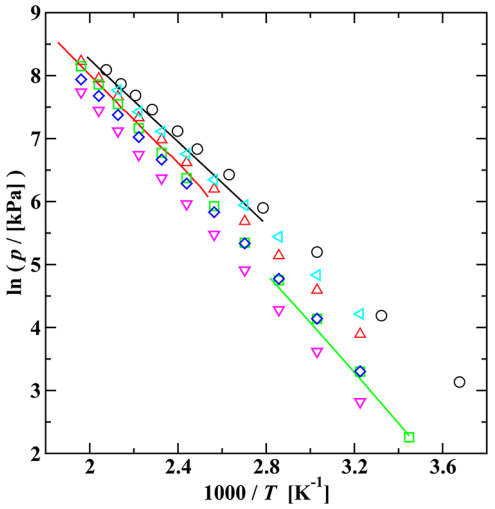

Figure 3. Clausius–Claperyon plots for cyclopentane, THF, and 1,3-dioxolane are shown as black circles, red triangles, and green squares, respectively, while the corresponding experimental data[59,61,62] are shown as solid lines. Data for THF using the Briggs, Girard, and Helfrich models are shown as blue diamonds, magenta down triangles, and cyan left triangles, respectively.

vapor pressures are somewhat overestimated by the TraPPE–UA model for all the molecules considered but become more accurate with increasing temperature. This overestimation of the vapor pressure at lower temperatures has been observed previously for united-atom models[11] and is likely due to a failure of united atoms to correctly describe the shape of alkyl groups. The use of an explicit-hydrogen model yields significantly improved vapor pressures for noncyclic alkanes but would significantly increase the computational cost.[11] Similarly, the use of anisotropic united-atom models can also lead to improved vapor pressures[26] but would also increase the computational cost and make the assignment of partial charges more difficult.

Since the development of the TraPPE–UA force field also emphasizes a good description of the dielectric properties of the liquid phase, there is an additional constraint, and one cannot shift the balance of LJ and dipole–dipole interactions to adjust the balance of enthalpy and entropy. The Briggs model underestimates the vapor pressures by a similar extent as the TraPPE–UA model overpredicts them. In contrast, the Girard and Helfrich models underpredict and overpredict, respectively, the vapor pressure by much larger amounts.

The critical constants and normal boiling temperatures for the five-membered rings are listed in Table 5. The critical

dx.doi.org/10.1021/jp302975c | J. Phys. Chem. B 2012, 116, 11234–11246

Table 5. Critical Constants and Normal Boiling Points

molecule	source	T_c [K]	ρ_c [kg/m^3]	T_b [K]
cyclopentane	TraPPE−UA	515.4 ± 2.7	282.6 ± 4.4	312.7 ± 0.9
	experiment[61]	511.7	270	322.4
THF	TraPPE−UA	544.4 ± 2.2	328.3 ± 4.3	330.8 ± 1.1
	Briggs	573.5 ± 3.0	320.1 ± 3.9	344.9 ± 0.9
	Girard	584.8 ± 2.3	315.6 ± 2.5	360.4 ± 1.1
	Helfrich	519.0 ± 2.7	256.0 ± 3.3	322.7 ± 0.9
	experiment[61]	541	320	339
1,3-dioxolane	TraPPE−UA	565.3 ± 2.7	389.1 ± 4.7	344.3 ± 0.9
	experiment[61]			347.7
cyclohexane	TraPPE−UA	553.8 ± 3.3	286.3 ± 3.9	342.8 ± 1.3
	experiment[61]	554	273	353.9
oxane	TraPPE−UA	584.1 ± 2.2	318.2 ± 3.3	361.2 ± 1.5
	experiment[61]	572.2	328	361
1,4-dioxane	TraPPE−UA	588.4 ± 3.0	369.2 ± 5.1	360.8 ± 1.0
	experiment[61]	587.3	369	374.3
1,3-dioxane	TraPPE−UA	606.5 ± 2.8	365.6 ± 4.6	374.6 ± 1.7
	experiment[61]			378.7
1,3,5-trioxane	TraPPE−UA	607.9 ± 2.3	430.9 ± 4.9	371.3 ± 1.6

Table 6. Comparison of Isothermal Compressibilities[55,63,64] and Heat Capacities[61] Determined Experimentally and Predicted by Simulation

molecule	κ^{sim}	κ^{expt}	C_p^{res}	C_p^{ideal}	C_p^{sim}	C_p^{expt}
	[GPa^{-1}]	[GPa^{-1}]	[J/(mol·K)]	[J/(mol·K)]	[J/(mol·K)]	[J/(mol·K)]
cyclopentane	1.58 ± 0.04	1.331	32 ± 2	90.7	123 ± 2	127.44
THF TraPPE−UA	1.14 ± 0.02	0.953	41 ± 2	83.0	124 ± 2	124.1
THF Briggs	0.96 ± 0.02	0.953	39 ± 1	83.0	122 ± 1	124.1
THF Girard	0.89 ± 0.02	0.953	43 ± 2	83.0	126 ± 2	124.1
THF Helfrich	1.69 ± 0.05	0.953	39 ± 2	83.0	122 ± 2	124.1
1,3-dioxolane	0.77 ± 0.03		50 ± 1	75.0	125 ± 1	120.84
cyclohexane	1.31 ± 0.03	1.130	35 ± 2	109.8	145 ± 2	154.2
oxane	0.96 ± 0.04	0.991	41 ± 2	101.1	142 ± 2	149.6
1,4-dioxane	0.80 ± 0.03	0.757	41 ± 2	95.0	136 ± 2	149.65
1,3-dioxane	0.79 ± 0.03	0.733	45 ± 2	93.1	138 ± 2	143.9
1,3,5-trioxane	0.63 ± 0.02		51 ± 2	84.4	135 ± 1	

temperatures for the TraPPE−UA model generally agree well with the experimental values,[61] but this should not come as a surprise because the LJ parameters are fitted to reproduce the critical temperatures. The critical densities are slightly overestimated for both cyclopentane and THF. As should be expected from the overprediction of the saturated vapor pressures, the normal boiling temperatures are underestimated by about 10 K, i.e., a similar extent as also found for linear alkanes.[9] However, the ratios of the predicted normal boiling temperatures (1.00:1.06:1.10) for cyclopentane, THF, and 1,3-dioxolane match the experimental ratios quite well (1.00:1.05:1.08). The Briggs and Girard models both overpredict the critical temperatures and the normal boiling points, though they give good agreement with the critical density, while the Helfrich model signficantly underpredicts all three properties.

The isothermal compressibilities and constant pressure heat capacities for the five-membered rings have been computed and are presented in Table 6. The simulations were all performed at 300 K and 1 atm to enable comparisons across the different models, but the experimental data were obtained at temperatures ranging from 293.15 to 303.15 K. In general, the experimental isothermal compressibilities are somewhat overpredicted for the TraPPE−UA model, though the ordering of the molecules is well reproduced. For this property, the Briggs and Girard THF models outperform the TraPPE−UA model, while κ for the Helfrich model is significantly too high. The TraPPE−UA model yields accurate predictions for the heat capacities of the five-membered rings with a mean unsigned deviation of 2% (and slight underprediction and overprediction for cyclopentane and 1,3-dioxolane, respectively). In contrast, the heat capacities for the six-membered rings are somewhat underpredicted with a mean signed deviation of 6%. For the cyclic alkanes, C_p^{ideal} is about three times larger than C_p^{res}, whereas the difference is less than a factor of 2 for 1,3-dioxolane and 1,3,5-trioxane and a factor of about 2 for the other oxygenated compounds. For THF, the differences in C_p^{res} for the four models agree within the statistical uncertainties.

Radial distribution functions (RDFs) for the five-membered rings are shown in Figure 4. The peaks in the center-of-mass RDFs shift to shorter distance with increasing number of oxygens, suggesting that the smaller size of oxygen, as well as the stronger dipole−dipole interactions between the oxygenated molecules, lead to more dense packing. For all three compounds, the center-of-mass RDF shows significantly more structuring (i.e., taller and narrower first peak and deeper first minimum) than any of the site−site RDFs. The strongly favorable Coulomb interactions between the oxygen atoms and

dx.doi.org/10.1021/jp302975c | J. Phys. Chem. B 2012, 116, 11234−11246

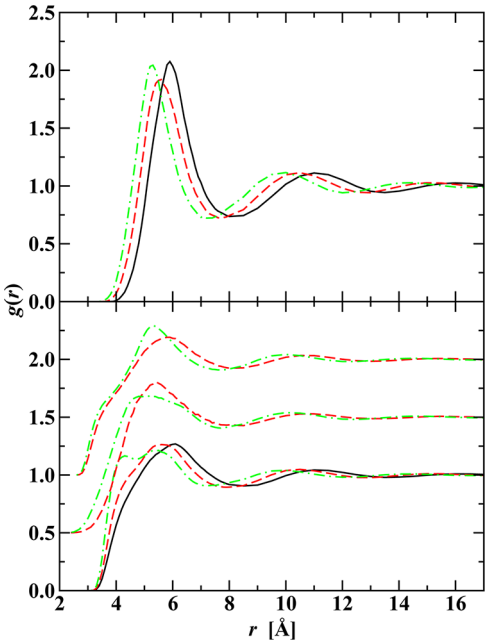

Figure 4. Center-of-mass (top) and site−site (bottom) radial distribution functions for five-membered rings. The COM−COM, C−C (unshifted), O−O (shifted up by 0.5 units), and O−C (shifted up by 1 unit) radial distribution functions are shown as black solid, red dashed, and green dot-dashed lines for cyclopentane, THF, and 1,3-dioxolane, respectively.

the α-methylene groups lead to a pronounced shoulder in the O−C RDFs of THF and 1,3-dioxolane. This feature is somewhat more pronounced for 1,3-dioxolane, and a splitting of the first peak in the C−C RDF is also found for this compound. This may be explained by a slightly greater preference for the formation of contacts between the more highly charged CH_2 group between the two oxygens in 1,3-dioxolane and an oxygen on a neighboring molecule.

The distributions of the mutual orientations of dipole vectors between a central molecule and those in its first solvation shell (which is bounded by the first minimum in the center-of-mass radial distribution function) are depicted in Figure 5. While both THF and 1,3-dioxolane exhibit only a very slight preference for parallel dipole alignment, the preference is somewhat more pronounced for THF, which is consistent with its slightly higher dipole moment (see below) and with the slightly higher peaks in the carbon−carbon and oxygen−oxygen RDFs.

The distributions of molecular dipole moments in both the vapor and liquid phases are shown in Figure 6. The average dipole moment of THF is 2.2 D, and there is only a single, symmetric peak in the dipole moment distribution. The distributions in the vapor and liquid phases are very similar with only a small shift to lower magnitudes for the vapor phase. The reason for the unimodal peak and the lack of sensitivity to the environment is due to the fact that the three atoms with the largest partial charges (the ether oxygen and the two α-methylene groups) form a fairly rigid unit, and changes in the conformation associated with torsional rotations have only a small effect on the dipole moment. For 1,3-dioxolane, on the other hand, the distributions are broad with two unresolved peaks. These peaks are of roughly equal height in the vapor phase, but there is a clear preference for the higher dipole conformation in the liquid phase. The average dipole moments

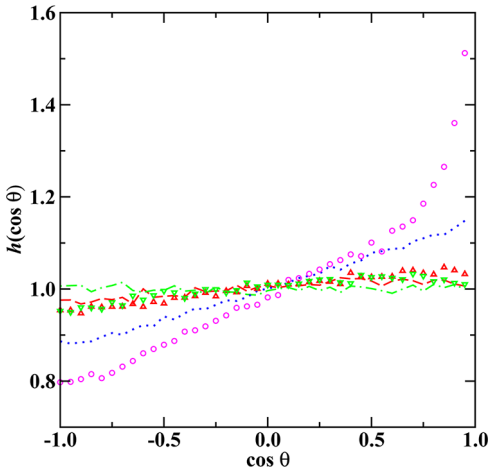

Figure 5. Distributions of the mutual dipole vector orientation with respect to neighboring molecules in the first solvation shell of THF, 1,3-dioxolane, oxane, 1,4-dioxane, 1,3-dioxane, and 1,3,5-trioxane are shown as a red dashed line, a green dot-dashed line, red up triangles, green down triangles, blue dots, and magenta circles, respectively.

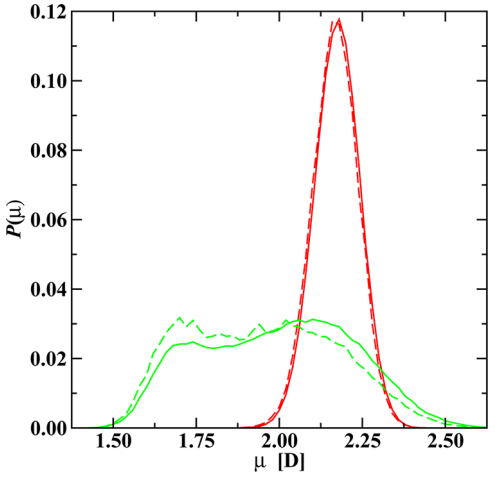

Figure 6. Distributions of the molecular dipole moments for THF (red) and 1,3-dioxolane (green) are depicted for the liquid phase (solid lines) and gas phase (dashed lines).

are 2.00 and 1.96 D for the liquid and vapor phase, respectively. The structure for the five-membered rings is fairly inflexible, but these two peaks correspond to folding different atoms out of the approximate plane of the ring. The conformational distribution in the vapor phase is governed by the torsional potential energy surface, whereas favorable dipole−dipole interactions in the liquid phase lead to a population shift to the conformers with higher dipole moment.

4.3. Vapor−Liquid Equilibria and Structural Data for Six-Membered Rings. The VLCCs for the six-membered rings are presented in Figure 7. The agreement with experimental data for cyclohexane[65] is very good with a slight underestimation of the density at low temperature. Few saturated liquid density data are available for the oxygenated compounds, but the densities for 1,4-dioxane and 1,3,5-trioxane agree fairly well with the correlations from Yaws.[60] The saturated liquid densities for 1,4-dioxane are slightly overestimated, while those for 1,3,5-trioxane are slightly underestimated. In addition, the ambient specific densities for oxane

dx.doi.org/10.1021/jp302975c | J. Phys. Chem. B 2012, 116, 11234−11246

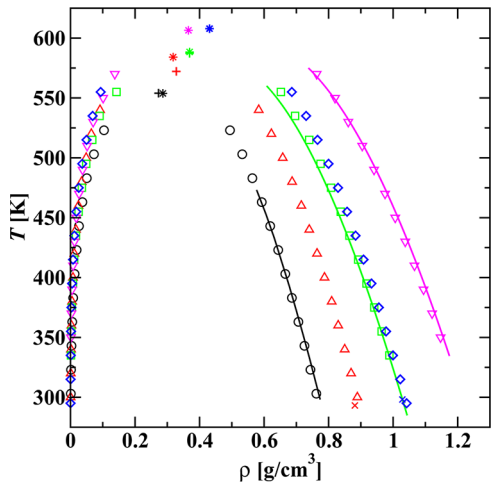

Figure 7. Vapor−liquid coexistence curves predicted by the TraPPE−UA force field for cyclohexane, oxane, 1,4-dioxane, 1,3-dioxane, and 1,3,5-trioxane are shown as black circles, red up triangles, green squares, blue diamonds, and magenta down triangles, respectively, while the corresponding experimental data[60,65] are shown as solid lines. Predicted and experimental critical points[61] are shown as stars and plus signs, respectively. The experimental liquid densities[55] for oxane and 1,3-dioxane are shown as red and blue crosses, respectively.

and 1,3-dioxane, while slightly overestimated, are in good agreement.

Clausius−Clapeyron plots for the six-membered rings are presented in Figure 8. The agreement with the available

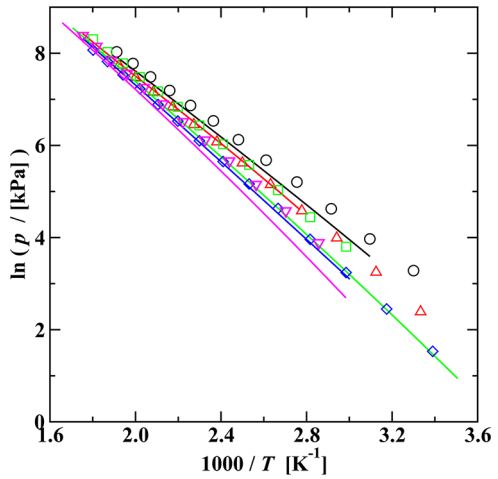

Figure 8. Clausius−Claperyon plots for cyclohexane, oxane, 1,4-dioxane, 1,3-dioxane, and 1,3,5-trioxane are shown as black circles, red up triangles, green squares, blue diamonds, and magenta down triangles, respectively, while the corresponding experimental data[60,61] are shown as solid lines.

data[61,60] is fairly good, particularly for oxane and 1,3-dioxane. For the other compounds, the vapor pressure is overestimated, particularly at low temperatures, as was observed for the five-membered rings. However, the order of the vapor pressure lines (in order of decreasing vapor pressure: cyclohexane, oxane, 1,4-dioxane, 1,3-dioxane, and 1,3,5-trioxane) is nearly reproduced by the TraPPE−UA force field with the 1,3,5-trioxane vapor pressure slightly higher than that for 1,3-dioxane.

The critical constants and normal boiling temperatures for the six-membered rings are summarized in Table 5. The critical temperatures generally agree well with the experimental[61] values, but T_c for oxane is overpredicted by 2%. The agreement for the critical densities is somewhat worse, with an overestimation of 5% for cyclohexane but a smaller discrepancy for oxane. The normal boiling temperatures are typically underestimated as expected from the overestimation of the vapor pressure, particularly at low temperatures. The exceptions are oxane and 1,3-dioxane for which the vapor pressure agreement was substantially better, and as a result, the boiling points are significantly closer. Compared to the five-membered rings, the TraPPE−UA force field correctly predicts that T_b for cyclohexane is slightly higher than that for 1,3-dioxolane. Overall, T_c, ρ_c, and T_b are predicted with mean unsigned percentage errors of 0.7, 3.0, and 2.0%. Since the underestimation of T_b is systematic, the mean signed percentage errors in this quantity match the corresponding unsigned errors. The isothermal compressibilities (see Table 6) are generally overestimated, though the relative ordering of the six-membered rings is well described. The heat capacities are underestimated, as for the five-membered rings.

Radial distribution functions for the six-membered rings are shown in Figure 9. As with the five-membered rings, the

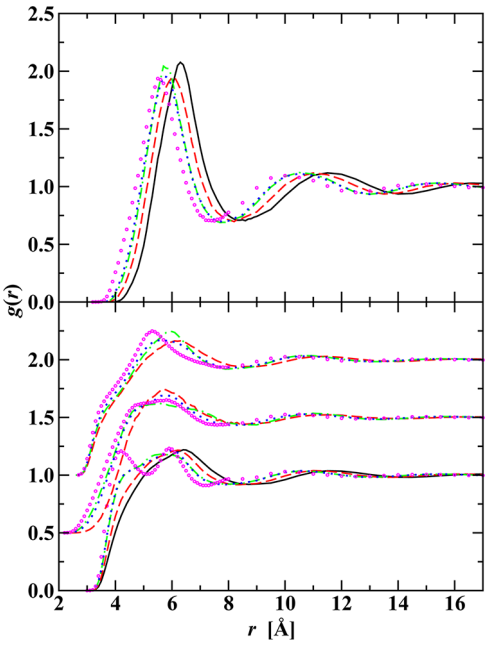

Figure 9. Center-of-mass (top) and site−site (bottom) radial distribution functions for six-membered rings. The COM−COM, C−C (unshifted), O−O (shifted up by 0.5 units), and O−C (shifted up by 1 unit) radial distribution functions are shown as black solid, red dashed, green dash-dotted, blue dotted lines, and magenta circles for cyclohexane, oxane, 1,4-dioxane, 1,3-dioxane, and 1,3,5-trioxane, respectively.

position of the first peak in the center-of-mass RDFs shifts to shorter separation with increasing number of oxygen atoms. For the two dioxanes, the center-of-mass RDFs nearly overlay, indicating that there is little difference in terms of overall packing between the two molecules. The first peak in the carbon−oxygen RDF is somewhat more pronounced for 1,4-dioxane, whereas the oxygen−oxygen RDF has a higher first peak for 1,3-dioxane. This may indicate that neighboring 1,4-dioxane molecules slightly prefer to form contacts between oxygen and carbon atoms or to orient oxygen toward the center

dx.doi.org/10.1021/jp302975c | J. Phys. Chem. B 2012, 116, 11234−11246

of the C−C bond; however, the difference in peak heights is small, and any differences in orientational preference are unlikely to be dramatic. As the number of oxygens increases, there is a small shoulder in the carbon−carbon radial distribution function at short separation for the dioxanes, and a distinct split is observed for 1,3,5-trioxane as orientational preferences may lead to distinct sets of preferred carbon−carbon distances.

The orientational correlation of the dipole moments for the six-membered rings in the first solvation shell is shown in Figure 5. There is virtually no correlation for 1,4-dioxane, which is expected due to the small dipole and only a very small preference for parallel orientations between neighboring dipoles in oxane. On the other hand, 1,3-dioxane and 1,3,5-trioxane have more ordered first solvation shells with a substantially higher probability for the molecular dipoles to be aligned. This alignment is consistent with the splitting of the first peak in the carbon−carbon RDF for 1,3,5-trioxane, as a given carbon atom on one of a pair of aligned molecules likely has one nearby carbon neighbor and two that are somewhat further away. These distinctions smear out for molecules with no particular orientational preference.

The distributions of molecular dipole moments in the vapor and liquid phases for the six-membered rings are shown in Figure 10. In general, these distributions exhibit a single peak,

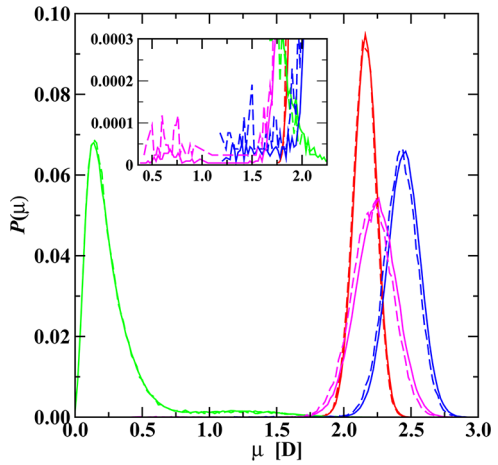

Figure 10. Distributions of the molecular dipole moments for oxane (red), 1,4-dioxane (green), 1,3-dioxane (blue), and 1,3,5-trioxane (magenta) are depicted for the liquid phase (solid lines) and gas phase (dashed lines). The inset shows a close-up of the region with intermediate dipole moments.

with its maximum at slightly higher dipole moments in the liquid phase than the vapor phase. The peak values for the dipole moments are 2.5, 2.25, and 2.15 D for 1,3-dioxane, 1,3,5-trioxane, and oxane, whereas the peak is located at 0.2 D for 1,4-dioxane. However, the distribution for 1,4-dioxane shows a secondary and very broad peak that results in an extended tail out to dipole moments of 2.1 D. Clearly, there are two main conformations with different dipole moments for 1,4-dioxane with the chair conformation yielding a small dipole moment and the boat conformation yielding a much enhanced dipole moment. There is also an extremely small secondary peak in the distributions for 1,3-dioxane and for 1,3,5-trioxane with dipole moments of about 1.5 and 0.7 D (see inset of Figure 10). These features of the distribution suggest that there may be higher-energy conformations that are populated under some conditions with a significantly different dipole moment. For six-membered rings, an equilibrium between boat and chair conformations seems the likely cause.

To investigate the boat/chair distribution in our simulations, it was necessary to develop a criterion to distinguish the two conformers. In the completely symmetric chair conformation of cyclohexane, each of the three pairs of atoms separated by three bonds can be linked by a line segment passing through the center of mass of the carbon atoms. For the boat conformation, this is roughly true for two of the pairs, while the third pair is situated significantly out of the plane. Therefore, for each of the six-membered rings, the midpoint of each 1−4 pair is determined, and the distances between these midpoints are calculated. A molecule is in the chair conformation if at least two of the distances between the midpoints are less than 0.25 Å and in the boat conformation if at least two of the distances between the midpoints are greater than 0.35 Å. This definition of boat and chair structures is somewhat ad hoc, but it describes the essential conformational features of the boat and chair structures and is not strongly sensitive to the precise choice of the cutoff distances. The populations of boat and chair conformations in the vapor and liquid phases have been computed for all five compounds and are summarized in Table 7. Note that a very small fraction of the molecules may satisfy neither conformational criterion, and hence, the sum of the two probabilities may not add to exactly one.

Table 7. Fraction of Boat and Chair Conformations

molecule	f_{liq}^{chair}	f_{liq}^{boat}	f_{vap}^{chair}	f_{vap}^{boat}
cyclohexane	0.995	0.004	0.996	0.004
oxane	0.984	0.013	0.985	0.012
1,4-dioxane	0.926	0.073	0.935	0.064
1,3-dioxane	0.961	0.038	0.963	0.035
1,3,5-trioxane	1.000	0.000	0.999	0.001

For all five molecules, the preference for the chair conformation is very pronounced in both vapor and liquid phases, but the two dioxanes have an appreciable boat population. There are likely two reasons for this. The first is that the torsional barriers for rotation around C−O bonds are generally lower than around C−C bonds, i.e., narrowing the energy penalty for the boat conformation. Second, for 1,4-dioxane and to a lesser degree 1,3-dioxane, the difference in populations between the vapor and liquid phases suggests that the boat conformer possesses a higher dipole moment, increasing the population of this conformation in the liquid phase where favorable dipole−dipole interactions are more important. For all of the molecules, except 1,4-dioxane, the difference between the boat populations in the vapor and liquid phases is negligible but, if anything, shows a slightly increased preference for the boat in the liquid phase. The exception is 1,3,5-trioxane, where the dipole moment for the boat structure seems to be lower as indicated by the long tail toward the small dipole moment in the distributions from Figure 10 and the population of the boat conformation is the lowest of all the six-membered rings.

4.4. Binary Mixtures. To assess the transferability of the newly developed parameters for cyclic alkanes and ethers, the vapor−liquid equilibria for binary mixtures of 1,3-dioxolane/cyclohexane and ethanol/1,4-dioxane were explored. The first case provides an opportunity to test the combination of parameters for the two different ring sizes considered here,

particularly the LJ parameters. In the second case, the effect of hydrogen bonding to the ether oxygen with its relatively small LJ diameter and large well depth is probed.

The results for the 1,3-dioxolane/cyclohexane mixture are shown in Figure 11. The bubble and dew point curves are

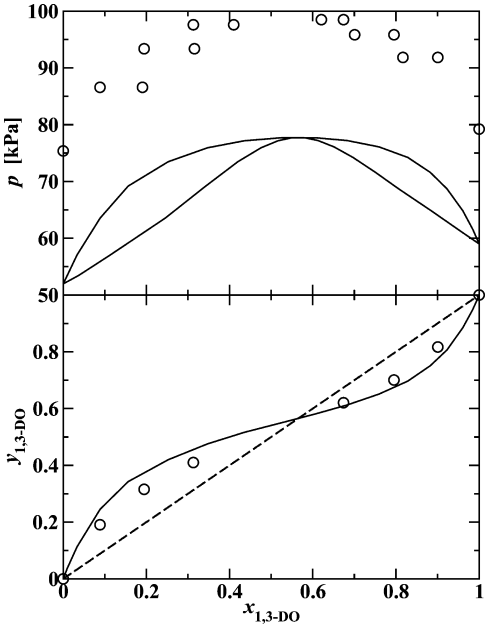

Figure 11. Pressure−composition diagram (top) and separation factor (bottom) for the vapor−liquid equilibria of the 1,3-dioxolane/cyclohexane mixture at T = 333.15 K. Simulation and experimental[66] data are shown as circles and solid lines, respectively.

shifted to higher pressures as should be expected from the vapor pressure results for the individual components. However, the shape of the pressure−composition curves is predicted quite well, and the concentration of the low-boiling azeotrope is near the experimental value.[66] The separation factors are slightly underestimated on both sides of the azeotrope.

The vapor−liquid coexistence data for the ethanol/1,4-dioxane mixture are depicted in Figure 12. The TraPPE−UA force field[13] is used for ethanol. The vapor pressure of the nonpolar 1,4-dioxane is significantly overestimated, whereas that of ethanol is fairly accurate. As a consequence, the upward shift of the bubble and dew point curves is lopsided with a much bigger shift at low ethanol concentrations. Although the presence of a low-boiling point azeotrope is predicted correctly, the composition of the azeotrope is significantly shifted toward 1,4-dioxane. However, the fact that the overall shape is in qualitative agreement with the experimental data[67] suggests that the strength of a hydrogen bond between a 1,4-dioxane acceptor and an ethanol donor molecule is reasonably well described. The boat and chair populations were computed to determine whether hydrogen bonding has a significant effect on the conformational preferences of 1,4-dioxane. However, the effect is fairly modest with a chair-conformer fraction of 0.966 for the 1,4-dioxane molecules in the liquid phase with the lowest nonzero ethanol mole fraction and a fraction of 0.961 for the phase with the highest ethanol mole fraction.

5. CONCLUSIONS

The TraPPE−UA force field was extended to five- and six-membered cyclic alkanes and ethers by fitting separate sets of

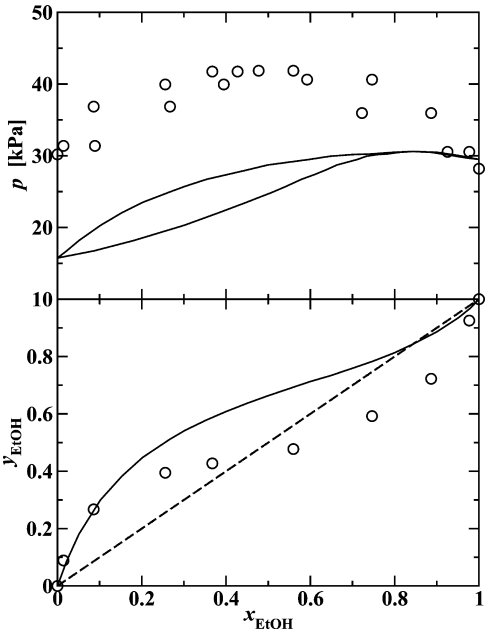

Figure 12. Pressure−composition diagram (top) and separation factor (bottom) for the vapor−liquid equilibria of the ethanol/1,4-dioxane mixture at T = 323.15 K. Simulation and experimental[67] data are shown as circles and solid lines, respectively.

LJ parameters for both ring sizes to vapor−liquid equilibria and concurrently adjusting the magnitude of the partial charges to reproduce the liquid-phase dielectric constants. This extension allows for the modeling of industrially important compounds and will be useful in applying the TraPPE−UA force field to simulations of carbohydrates. A Monte Carlo based simulated annealing procedure was applied to allow simultaneous fitting of multiple types of torsional potentials in the same and in different molecules.

The TraPPE−UA model yields excellent agreement for liquid densities and critical temperatures with mean unsigned percentage errors of less than 1%, whereas the saturated vapor pressures are significantly overestimated particularly at low temperatures and the mean unsigned percentage error for the normal boiling temperature is 2%.

The presence of oxygen atoms in these cyclic compounds leads to large increases in the liquid density and shifts the radial distribution functions toward shorter separations, likely as a result of favorable dipole−dipole interactions and the deeper LJ well and smaller LJ size of the oxygen atom compared to the CH_2 united atom. In general, there is some mutual alignment of neighboring dipoles for the oxygenated rings, though except for 1,3-dioxane and 1,3,5-trioxane this preference is slight. For all six-membered rings, the chair conformation is strongly preferred. However, the dioxane compounds exhibit somewhat higher populations of the boat conformation than the other compounds because torsional rotation around C−O bonds is typically associated with lower-energy penalties than around C−C bonds and also because the boat conformation has a higher dipole moment particularly for 1,4-dioxane. For 1,3,5-trioxane, the boat structure possesses a smaller dipole moment. In general, the conformer populations and distributions of dipole moments are quite similar in the vapor and liquid phases. The exception is 1,3-dioxolane where the conformer population is significantly shifted toward those with higher dipole moments in the liquid phase.

Good qualitative agreement is also obtained for the vapor−liquid equilibria of the binary 1,3-dioxolane/cyclohexane and ethanol/1,4-dioxane. Both binary mixtures yield a low-boiling azeotrope.

■ ASSOCIATED CONTENT

Supporting Information

Complete author list for reference 5. The numerical data for all of the figures shown in this article are available as electronic files. This is a tar archive containing the ASCII text files produced by the Grace plotting program (http://plasma-gate.weizmann.ac.il/Grace/). This material is available free of charge via the Internet at http://pubs.acs.org.

■ AUTHOR INFORMATION

Corresponding Author

*E-mail: siepmann@umn.edu.

Notes

The authors declare no competing financial interest.

■ ACKNOWLEDGMENTS

Financial support from the National Science Foundation (CBET-0756641 and CBET-1159837) and from the Abu Dhabi−Minnesota Institute for Research Excellence (ADMIRE), a partnership between the Petroleum Institute of Abu Dhabi and the Department of Chemical Engineering and Materials Science of the University of Minnesota, is gratefully acknowledged. Part of the computer resources were provided by the Minnesota Supercomputing Institute.

■ REFERENCES

(1) Speight, J. G. *Handbook of Petroleum Analysis*; Wiley-Interscience: New York, NY, 2001.
(2) Siepmann, J. I. *NIST Spec. Publ.* **2001**, *975*, 110−112.
(3) Weiner, S. J.; Kollman, P. A.; Nguyen, D. T.; Case, D. A. *J. Comput. Chem.* **1986**, *7*, 230−252.
(4) Jorgensen, W. L.; Maxwell, D. S.; Tirado-Rives, J. *J. Am. Chem. Soc.* **1996**, *118*, 11225−11236.
(5) MacKerell, A. D.; Bashford, D.; Bellott, M.; Dunbrack, R. L.; Evanseck, J. D.; Field, M. J.; Fischer, S.; Gao, J.; Guo, H.; Ha, S.; et al. *J. Phys. Chem. B* **1998**, *102*, 3586−3616.
(6) Oostenbrink, C.; Villa, A.; Mark, A. E.; van Gunsteren, W. F. *J. Comput. Chem.* **2004**, *25*, 1656−1676.
(7) Perez-Pellitero, J.; Bourasseau, E.; Demachy, I.; Ridard, J.; Ungerer, P.; Mackie, A. D. *J. Phys. Chem. B* **2008**, *112*, 9853−9863.
(8) Vahid, A.; Sans, A. D.; Elliott, J. R. *Ind. Eng. Chem. Res.* **2008**, *47*, 7955−7964.
(9) Martin, M. G.; Siepmann, J. I. *J. Chem. Phys.* **1998**, *102*, 2569−2577.
(10) Martin, M. G.; Siepmann, J. I. *J. Phys. Chem. B* **1999**, *103*, 4508−4517.
(11) Chen, B.; Siepmann, J. I. *J. Phys. Chem. B* **1999**, *103*, 5370−5379.
(12) Wick, C. D.; Martin, M. G.; Siepmann, J. I. *J. Phys. Chem. B* **2000**, *104*, 8008−8016.
(13) Chen, B.; Potoff, J. J.; Siepmann, J. I. *J. Phys. Chem. B* **2001**, *105*, 3093−3104.
(14) Stubbs, J. M.; Pottoff, J. J.; Siepmann, J. I. *J. Phys. Chem. B* **2004**, *108*, 17596−17605.
(15) Wick, C. D.; Stubbs, J. M.; Rai, N.; Siepmann, J. I. *J. Phys. Chem. B* **2005**, *109*, 18974−18982.
(16) Lubna, N.; Kamath, G.; Potoff, J. J.; Rai, N.; Siepmann, J. I. *J. Phys. Chem. B* **2005**, *109*, 24100−24107.
(17) Rai, N.; Siepmann, J. I. *J. Phys. Chem. B* **2007**, *111*, 10790−10799.
(18) Maerzke, K. A.; Schultz, N. E.; Ross, R. B.; Siepmann, J. I. *J. Phys. Chem. B* **2009**, *113*, 6415−6425.
(19) Maerzke, K.; Siepmann, J. I. *J. Phys. Chem. B* **2011**, *115*, 3452−3465.
(20) Lee, J.-S.; Wick, C. D.; Stubbs, J. M.; Siepmann, J. I. *Mol. Phys.* **2005**, *103*, 99−104.
(21) Ketko, M.-B. H.; Rafferty, J. L.; Siepmann, J. I.; Potoff, J. J. *Fluid Phase Equilib.* **2008**, *274*, 44−49.
(22) Yazaydin, A. O.; Thompson, R. W. *Mol. Simul.* **2006**, *32*, 657−662.
(23) Vorobyov, I.; Anisimov, V. M.; Greene, S.; Venable, R. M.; Moser, A.; Pastor, R. W.; MacKerell, A. D. *J. Chem. Theory Comput.* **2007**, *3*, 1120−1133.
(24) Jalkanen, J. P.; Pakkanen, T. A.; Rowley, R. L. *J. Chem. Phys.* **2004**, *120*, 1705−1714.
(25) Errington, J. R.; Panagiotopoulos, A. Z. *J. Chem. Phys.* **1999**, *111*, 9731−9738.
(26) Borasseau, E.; Ungerer, P.; Boutin, A. *J. Phys. Chem. B* **2002**, *106*, 5483−5491.
(27) Milano, G.; Müller-Plathe, F. *J. Phys. Chem. B* **2004**, *108*, 7415−7423.
(28) B. Eckl, J.; Vrabec, H. H. *J. Phys. Chem. B* **2008**, *112*, 12710−12721.
(29) Chanrasekhar, J.; Jorgensen, W. L. *J. Chem. Phys.* **1982**, *77*, 5073−5079.
(30) Helfrich, J.; Hentschke, R. *Macromolecules* **1995**, *28*, 3831−3841.
(31) Jorgensen, W. L.; Madura, J. D.; Swenson, C. J. *J. Am. Chem. Soc.* **1984**, *106*, 6639−6646.
(32) Girard, S.; Müller-Plathe, F. *Mol. Phys.* **2003**, *101*, 779−787.
(33) Geerlings, J. D.; Varma, C. A. G. O.; van Hemert, M. C. *J. Phys. Chem. B* **2000**, *104*, 56−65.
(34) Krienke, H.; Ahn-Ercan, G.; Barthel, J. *J. Mol. Liq.* **2004**, *109*, 115−124.
(35) Maitland, G. C.; Rigby, M.; Smith, E. B.; Wakeham, W. A. *Intermolecular Forces: Their Origin and Determination*; Pergamon Press: Oxford, 1987.
(36) Perdew, J. P. *Phys. Rev. B* **1992**, *46*, 6671−6687.
(37) Mulliken, R. S. *J. Chem. Phys.* **1955**, *23*, 1833−1840.
(38) Guvench, O.; MacKerell, A. D. *J. Mol. Model.* **2008**, *14*, 667−679.
(39) Panagiotopoulos, A. Z. *Mol. Phys.* **1987**, *61*, 813−826.
(40) Panagiotopoulos, A. Z.; Quirke, N.; Stapleton, M.; Tildesley, D. J. *Mol. Phys.* **1988**, *63*, 527−545.
(41) Siepmann, J. I.; Frenkel, D. *Mol. Phys.* **1992**, *75*, 59−70.
(42) Vlugt, T. J. H.; Martin, M. G.; Smit, B.; Siepmann, J. I.; Krishna, R. *Mol. Phys.* **1998**, *94*, 727−733.
(43) Mooij, G. C. A. M.; Frenkel, D.; Smit, B. *J. Phys.: Condens. Matter* **1992**, *4*, L255−L259.
(44) Wick, C. D.; Siepmann, J. I. *Macromolecules* **2000**, *33*, 7207−7218.
(45) Wood, W. W.; Parker, F. R. *J. Chem. Phys.* **1957**, *27*, 720−733.
(46) Ewald, P. *Ann. Phys.* **1921**, *64*, 253−287.
(47) Madelung, E. *Phys. Z.* **1918**, *19*, 524−532.
(48) Allen, M. P.; Tildesley, D. J. *Computer Simulation of Liquids*; Oxford University Press: New York, NY, 1987.
(49) Rowlinson, J. S.; Widom, B. *Molecular Theory of Capillarity*; Oxford University Press: New York, NY, 1989.
(50) Rowlinson, J. S.; Swinton, F. L. *Liquids and Liquid Mixtures*; Butterworth: London, 1982.
(51) Atkins, P. W.; de Paula, J. *Physical Chemistry*, 7th ed.; W. H. Freeman and Company: New York, NY, 2002.
(52) McDonald, I. R. *Mol. Phys.* **1972**, *23*, 41−58.
(53) McQuarrie, D. A. *Statistical Mechanics*; University Science Books: Virginia, 2000.
(54) NIST Computational Chemistry Comparison and Benchmark Database, NIST Standard Reference Database Number 101; Johnson, R.D., III, Ed.; National Institute of Standards and Technology: Gaithersburg, MD 20899 (http://srdata.nist.gov/cccbdb).

(55) *CRC Handbook of Chemistry and Physics*, 88th ed.; Lide, D. R., Baysinger, G., Berger, L. I., Goldberg, R. N., Kehiaian, H. V., Kuchitsu, K., Rosenblatt, G., Roth, D. L., Zwillinger, D., Eds.; CRC Press: Boca Raton, FL, 2007.
(56) Venkateswaran, A.; Easterfield, J. R.; Davidson, D. W. *Can. J. Chem.* **1967**, *45*, 884−886.
(57) Walker, R.; Davidson, D. W. *Can. J. Chem.* **1959**, *37*, 492−495.
(58) Briggs, J. M.; Matsui, T.; Jorgensen, W. L. *J. Comput. Chem.* **1990**, *11*, 958−971.
(59) Vargaftik, N. B. *Tables on the Thermophysical Properties of Liquids and Gases*; Hemisphere Publishing Company: Washington D.C., 1975.
(60) Yaws, C. L. *Yaws' Thermophysical Properties of Chemicals and Hydrocarbons*; Knovel: Norwich, NY, 2009.
(61) NIST Chemistry WebBook, NIST Standard Reference Database Number 69; Linstrom, P.J., Mallard, W.G., Eds.; National Institute of Standards and Technology: Gaithersburg MD, 20899 (http://webbook.nist.gov).
(62) Kobe, K. A.; Ravicz, A. E.; Vohra, S. P. *Ind. Eng. Chem.* **1956**, *1*, 50−56.
(63) Takigawa, T.; Tamura, K. *J. Chem. Thermodyn.* **2000**, *32*, 1045−1055.
(64) Moelwyn-Hughes, E. A.; Thorpe, P. L. *Proc. R. Soc. London A* **1964**, *278*, 574−587.
(65) Beg, S. A.; Tukur, N. M.; Al-Harbi, D. K.; Hamad, E. Z. *J. Chem. Eng. Data* **1993**, *38*, 461−464.
(66) Wu, H. S.; Sandler, S. I. *J. Chem. Eng. Data* **1989**, *34*, 209−213.
(67) González, J. A.; Mozo, I.; Fuente, I. G. D. L.; Cobos, J. C.; Durov, V. A. *Fluid Phase Equilib.* **2006**, *245*, 168−184.